Accepted Manuscript

Volume 17
Number 1
7 January 2017
Pages 1-200

Lab on a Chip

Devices and applications at the micro- and nanoscale

rsc.li/loc

ISSN 1473-0197

ROYAL SOCIETY OF CHEMISTRY

PAPER
Chengzhi Hu, Bradley J. Nelson et al.
Characterization of size-dependent mechanical properties of top-growing cells using a lab-on-a-chip device
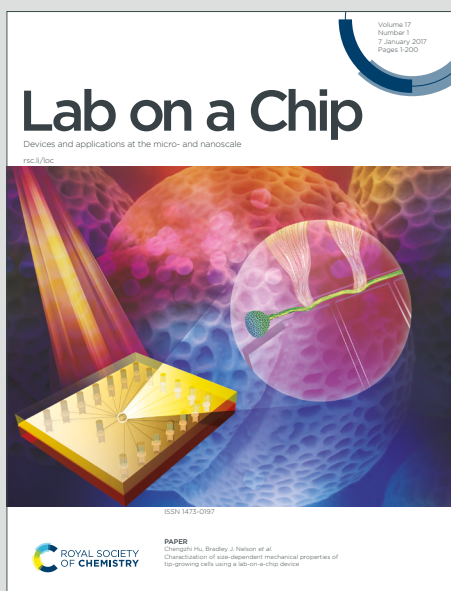
This is an Accepted Manuscript, which has been through the Royal Society of Chemistry peer review process and has been accepted for publication.

Accepted Manuscripts are published online shortly after acceptance, before technical editing, formatting and proof reading. Using this free service, authors can make their results available to the community, in citable form, before we publish the edited article. We will replace this Accepted Manuscript with the edited and formatted Advance Article as soon as it is available.

You can find more information about Accepted Manuscripts in the Information for Authors.

Integration of Paper Microfluidic Sensors into Contact Lenses for Tear Fluid Analysis

Rosalia Moreddu,[1,2,] Mohamed Elsherif,[3] Hadie Adams,[4] Maria F. Cordeiro,[5] James S. Wolffsohn,[6] Daniele Vigolo,[2] Haider Butt,[7] Jonathan M. Cooper,[8] Ali K. Yetisen[1]*

[1]Department of Chemical Engineering, Imperial College London, London SW7 2AZ, United Kingdom

[2]School of Chemical Engineering, University of Birmingham, Birmingham B15 2TT, United Kingdom

[3]Department of Experimental Physics, Nuclear Research Center, Egyptian Atomic Energy Authority, Cairo 11865, Egypt

[4]Department of Medicine, Imperial College London, London SW7 2AZ, United Kingdom

[5]The Western Eye Hospital, Imperial College Healthcare NHS Trust, London, NW1 5QH UK

[6]School of Life and Health Sciences, Aston University, Birmingham, B4 7ET, United

Kingdom

[7]Department of Mechanical Engineering, Khalifa University, Abu Dhabi 127788, United

Arab Emirates

[8]Division of Biomedical Engineering, School of Engineering, University of Glasgow,

Glasgow G12 8LT, United Kingdom

*r.moreddu18@imperial.ac.uk

Abstract

In this article, using the integration of paper microfluidics within laser-inscribed commercial

contact lenses, we demonstrate the multiplexed detection of clinically relevant analytes including

hydrogen ions, proteins, glucose, nitrites and L-ascorbic acid, all sampled directly from model tears. *In vitro* measurements involved the optimization of colorimetric assays, with readouts collected, stored and analyzed using a bespoke Tears Diagnostics smartphone application prototype. We demonstrate the potential of the device to perform discrete measurements either for medical diagnosis or disease screening in the clinic or at the point-of-care (PoC), with future applications including monitoring of ocular infections, uveitis, diabetes, keratopathies and assessing oxidative stress.

Introduction

Diagnostic devices that can monitor metabolites in body fluids have the potential to revolutionize healthcare.[1] It has been validated that the detection of such analytes can enable opportunities both for disease screening and early-stage diagnostics using affordable technologies that can be operated by non-specialists in clinical or point-of-need settings.[2-5] Despite being an easily accessible organ, the physiology of the eye poses diagnostic challenges. Recent advances have been made towards the investigation of the composition of tears as a potential medium to monitor ocular health.[6, 7] Tears reflect both ocular and systemic physiological states by expressing a variety of biomarkers, as proxies either for chronic or acute disease (including infections) as well as local trauma or injury. They nourish the ocular proximal tissues and it contributes towards regulating corneal homeostasis. The "proximal fluid" is the final output of the lacrimal function unit, facing the external environment.[8]

Tears are complex fluids comprising a mixture of lipids, electrolytes, proteins, peptides, glucose and amino-acids. In general, the composition dynamically reflects the physiological state, including levels of hydration, infection and general well-being. For example, whilst the normal protein concentration in tears lies in the range 3-7 mg mL^{-1},[9] recent reports in tear proteomics has enabled the diagnosis of diabetic retinopathy, aniridia,[10] keratopathies, and dry eye[11] (for example, a two-fold decrease in protein levels is reported in keratopathic tears when compared to healthy controls.)

Vitamins C, A, E and those in the B family are also found in tears. In particular, ocular tissues and fluids contain high levels of L-ascorbic acid (vitamin C)[12] which plays a role

in antioxidant protection,[13] wound healing and inflammatory processes in the cornea.[14] In patients undergoing early-stage corneal damage, it has been argued that leakages of ascorbic acid from the corneal epithelial cells may be found in the tear films, making it a potential biomarker for corneal disorders, alkali burns,[15] and inflammation after excimer laser corneal surgery.[16] Thus in general the tear ascorbate levels can be related to the corneal health status.

Current techniques for pH measurement have included micro-combination glass probes,[17] and microelectrodes[18] inserted in the eye, showing that the healthy tear pH ranges from 6.0 to 7.6.[17] Tear pH is crucial with regards to the ocular penetration of drugs[18] and in the early diagnosis of ocular rosacea (where the tear pH of non-treated ocular rosacea patients was found to be 8.0 ± 0.32, compared to 7.0 ± 0.18 in healthy controls).[19] Tear pH was also found to increase in pre- and post-operative senile cataract patients, resulting in pH values ranging from 7.26 ± 0.23 on the day before the operation to 7.50 ± 0.23 on the first post-operative day.[20]

Nitric oxide is an important mediator of homeostatic processes in the eye, such as regulation of aqueous humour dynamics, retinal neurotransmission, and phototransduction.[21] Changes in its generation or action may be associated with diverse inflammatory states, including uveitis, retinitis, Behçet's syndrome, and degenerative diseases such as glaucoma. These variations can be monitored by measuring tear nitrites as nitric oxide by-products. Healthy tears were reported to have nitrite levels of the order of 110-120 µmol L^{-1},[21] compared to the values of near 80 µmol L^{-1} in uveitis patients.[21] In uveitis patients, both with and without ocular complications, tear nitric

oxide was found to quickly oxidize in peroxynitrite, a highly oxidizing cytotoxic substance.[21] Nitrites and nitrates levels as nitric oxide cytotoxic end products were found to significantly decrease in active Behçet's patients, with average concentrations of 82.3 μmol L^{-1}.

Tear fluid has previously been extensively investigated as an alternative body fluid for the monitoring of body sugar levels in diabetic patients.[22, 23] The correlation between tear glucose and capillary blood glucose can allow for the assessment of the diabetic status of a subject exclusively using tear glucose values.[22, 24, 25] Examples of technologies used in the development of tear glucose sensors are glucose-sensitive photonic crystals,[26] holographic sensors[6] and molecularly-imprinted fluorescent sensors.[27] Glucose sensitive-contact lenses have also been proposed,[28, 29] although it is noted that in some cases, these methods are often based upon electrical readouts, do not operate within normal physiological ranges, and their readout mechanisms are impracticable or unfeasible.[30-32]

Currently, tear screening is performed clinically as a three-steps process involving tear sampling, sample extraction from the medium, and analysis. Tears are normally sampled by capillarity using a Schirmer's paper strip inserted in the lower eyelid for 5 minutes, then extracted and analyzed in a laboratory. The drawbacks of the Schirmer's test are the length of the process, the contamination risks associated with sample extraction, and the tear overflow induced by irritation (with analyte dilution). It has also been shown that irritation associated with sampling induces compositional variations.[9] As a consequence, currently analysis can be only performed by healthcare professionals.

The method that we report here addresses these shortcomings offering a platform with the potential to perform both *in situ* tear fluid analysis together with the multiplexed integration ofchemical sensors for the simultaneous measurement of biomarkers/proxies for clinical problems (i.e.

glucose, proteins, ascorbic acid, nitrite ions and pH). The current literature indicates that although paper microfluidics has been used in wearable devices (e.g. for sweat monitoring),[33, 34] its use through integration into a contact lens is yet to be explored. Similarly, whilst paper microfluidics has been used for in vitro (*ex situ*) tear sampling, e.g. Schirmer's paper strip and paper microfluidic devices,[34] the integration of this technology into a contact lens has not yet been reported.

By adopting a paper-based microfluidic approach into contact lenses we were able to minimize leakage and facilitate capillary flow within the system (**Figure 1**). The device was manufactured using laser ablation of contact lenses and laser cutting of paper microchannels (**Figure 1a**). Paper-embedded biochemical sensors were integrated within the microfluidic lenses (**Figure 1b**). The system was finally enclosed using a poly-HEMA lab-made contact lens as a top layer which was chemically bonded to seal the device. The inlet allows tear fluid to flow form the concave side of the contact lens into the microchannel. A smartphone-based readout method was used to collect and store information, enabling on-eye discrete direct collection and detection of analytes from the tear (**Figure 1c**).
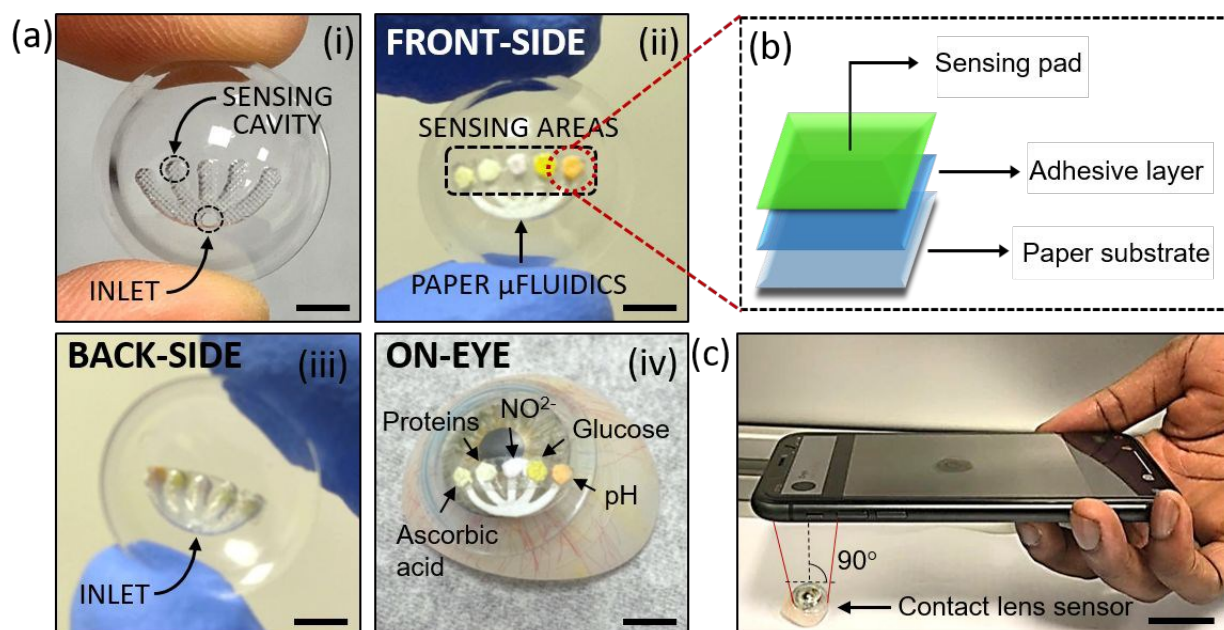
Figure 1. *Microfluidic contact lens sensor. (a) Device fabrication: (i) Laser-inscribed microfluidic system in a contact lens; (ii) Embedding the paper microfluidic chip within the contact lens; (iii) Backside view of the contact lens sensor; (iv) Contact lens sensor on an artificial eye model. Scale bars: 1.5 cm. (b) Schematic of the structure of each sensing area; (c) Representative photograph of the readout method. Scale bar: 2.0 cm.*

Results and Discussion

Chemical sensors immobilized within paper matrices were embedded within microfluidic contact lens structures in order to detect tear pH, glucose, proteins, L-ascorbic acid, and nitrites in the physiological range. Upon changing the concentration of tear analytes, the chromogenic sensors yielded a variation in the primary reflected wavelength within the visible spectrum. pH sensors, based on methyl red and bromothymol blue, responded to the range between pH 5.0 to 8.0 (**Figure 2a**) providing a color shift from orange (pH 5.0) to yellow (pH 6.0) and green (7.0-8.0). Organic methyl red sensed acidic pH variations from 4.0 to 6.0 via its carboxylic and amine functional

groups. Intermediate pH values (6.0-8.0) were detected by bromothymol blue, a weak acid that forms triphenylmethane in alkaline media. **Figure 2b** shows the reflection spectra of tear pH sensors. The corresponding calibration curve with a linear fitting (R^2= 0.99) is shown in **Figure 2c**. The sensors yielded a sensitivity of 22 nm/pH units, and a Limit of Detection (LOD) of 0.13 pH units in the physiological range 7.0 - 8.0. The colors associated to discrete concentration values were uniquely identified with their X, Y coordinates in the CIE 1931 chromaticity diagram, shown in **Figure 2d**. To each X, Y pair is associated an RGB triplet which was acquired with a smartphone camera and back-calculated from the X, Y pairs. The percentage of RGB colors over the pH value is shown in **Supplementary Figure S1a**, where a decrease in the color intensity was observed upon increasing the pH, as well as a decrease in the red contribution when shifting from orange to green. The pH sensor had a response time of 15 s, that remained stable for the following 10 s as shown in **Figure 2e** for pH 6.0, 7.0, and 8.0. **Supplementary Figure S3** shows the reflection spectra over time when exposing the sensors to pH buffers of 6.0, 7.0, and 8.0.

To evaluate the stability of the sensors under UV light, which may be of interest in the

case of continuous monitoring applications, the sensors were exposed to artificial UV light

at 355 nm to emulate the sun exposure of the eye. They yielded a stable behavior up to

30 minutes of exposure (**Figure 2f**), with a stable reflection peak around 550 nm,

corresponding to the imaged green color (**Supplementary Figure S2a**).
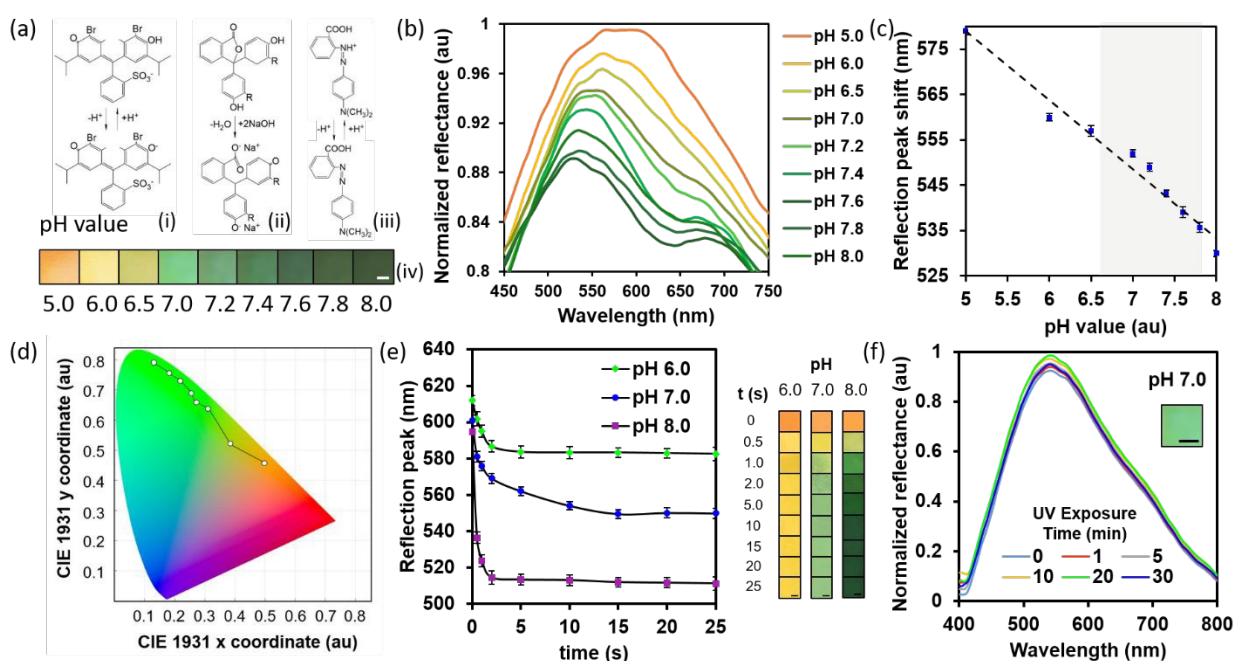
Figure 2. Characterization of the paper tear pH sensor over the range between 5.0 and

8.0: (a) shows the sensing mechanism of hydrogen ions; (i) Bromothymol Blue; (ii)

Phenolphthalein; (iii) Methyl red; (iv) Photographs of the chromogenic sensors; scale bar: 1.5

mm. (b) Normalized reflection spectra between pH 5.0 to 8.0; (c) Calibration curve of the

pH sensor (with the grey area highlighting the physiological range); (d) Chromaticity diagram of the pH sensor, displaying the color change from pH 5.0 to pH 8.0. (e) Time response of the pH sensor when exposed to buffer solutions at pH 6.0, 7.0 and 8.0. The inset figure shows the color change within 25 seconds. Scale bars: 1.0 mm. (f) Influence of UV exposure from 0 to 30 minutes at pH 7.0; inset scale bar: 1.5 mm.

Glucose sensors were produced based on the glucose oxidase (GOD)/peroxidase (POD) method, comprising of GOD, POD, and 3,3′,5,5′-tetramethylbenzidine (TMB) (**Figure 3a**). Ambient oxygen oxidized β-D-glucose to D-gluconolactone, producing hydrogen peroxide which in turn oxidized TMB under peroxidase catalysis. **Figure 3b** displays the reflection spectra of the glucose sensors at different glucose concentrations (0 to 10.0 mmol L^{-1}). The reflection wavelength peak at 580 nm decreased upon increasing glucose concentration in artificial tears to 10.0 mmol L^{-1}. The calibration curve in **Figure 3c** could be approximated with a linear fitting (R^2=0.93), with a sensitivity of 3.9 nm/mmolL^{-1} and a LOD of 1.1 mmolL^{-1}. As explained for the pH sensor, **Figure 3d** shows the CIE 1931 chromaticity diagram of the calibration points corresponding to the color of the glucose sensor at different glucose concentrations. **Supplementary Figure S1b** shows the RGB values of glucose sensors in the range 0 to 10.0 mmol L^{-1}.

The response time of the glucose sensor was 15 s, measured at concentrations of 2, 5 and 10 mmolL^{-1} (**Figure 3e**). **Supplementary Figure S4** displays the reflection spectra over time at glucose concentrations of 2, 5 and 10 mmolL^{-1}. The glucose sensor showed good stability when

exposed to UV light up to 30 minutes, with consistent reflection peaks and colors (**Figure 2f,**

Supplementary Figure S2b).
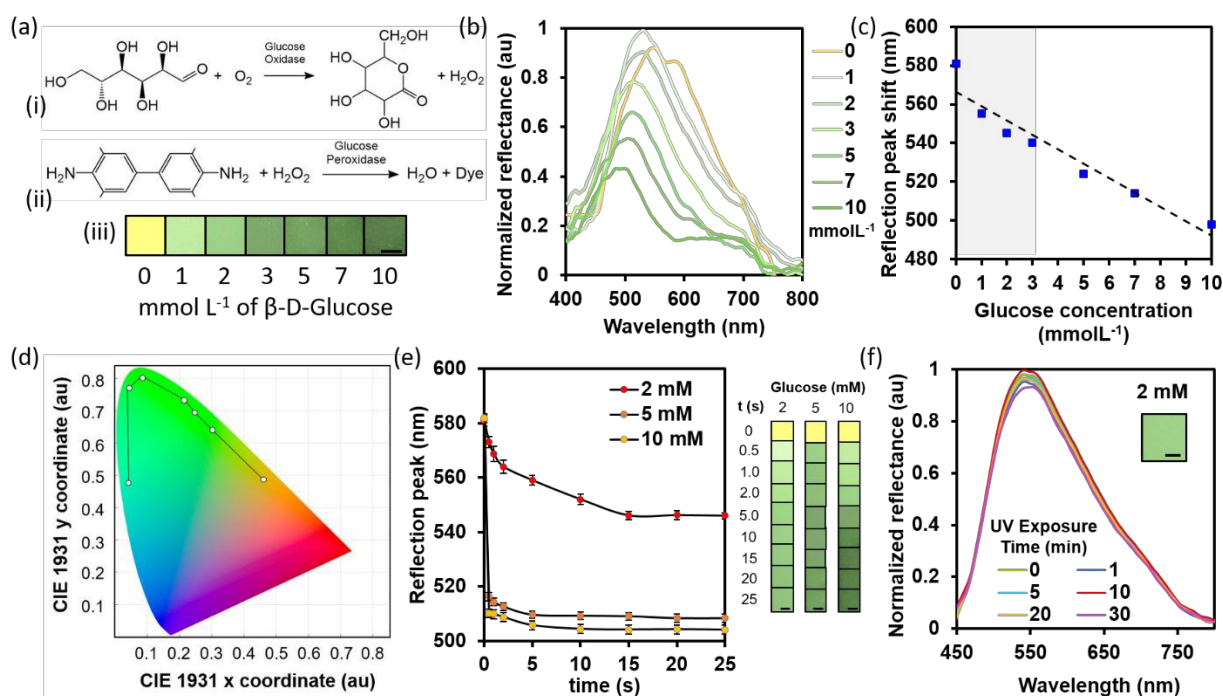
Figure 3. *Characterization of the paper tear glucose sensor in the range between 0 and*

10 mmolL⁻¹. (a) shows the sensing mechanism of β-D-glucose: (i) Formation of hydrogen

peroxide from glucose and ambient oxygen, in the presence of glucose oxidase; (ii)

3,3',5,5'-Tetramethylbenzidin reacts with hydrogen peroxide in the presence of glucose peroxidase

to form a dye. (iii) Photographs of the chromogenic sensor; scale bar: 1.5 mm. (b)

Normalized reflection spectra of the glucose sensor at different concentrations; (c)

Calibration curve of the glucose sensor (with the grey area highlighting the physiological

range); (d) Chromaticity diagram of the glucose sensor, displaying the color change with

glucose concentration from 0 to 10.0 mmolL^{-1}. (e) Time-dependent reflection peak shift

when exposed to 2.0 mM, 5.0 mM and 10 mM glucose solution. The inset figure shows

the color shift over time. Scale bars: 1.0 mm. (f) UV-dependent behavior of the glucose

sensor at a glucose concentration of 2.0 mmolL^{-1}. Inset scale bar: 1.5 mm.

Protein sensors detected bovine serum albumin (BSA) concentrations from 0 to 8.0 mg mL^{-1} (**Figure 4**) and they were based on 3′,3″,5′,5″-tetrachlorophenol-3,4,5,6-tetrabromosulfophthalein, which interact with the proteins functional groups leading to protonation/deprotonation with consequent displacement of the π-electron system, exhibiting a color shift from yellow to green upon variations in protein concentration from 0 to 8.0 mg mL^{-1}. **Figure 4b** shows the absorbance spectra of protein sensors, displaying an increase in the reflection intensity upon variations in the protein concentration from 0.0 to 8.0 mg mL^{-1}, which corresponded to increasingly brighter colors. The calibration curve is shown in **Figure 4c**, approximated by a linear fitting (R^2=0.98) and giving a sensitivity of 2.1 nm mL^{-1} and a LOD of 1.1 mg mL^{-1}. **Figure 4d** shows the CIE 1931 chromaticity plot of the protein sensors, which displayed the discrete calibration points obtained

by measuring the color change with variation in protein concentration. The RGB characterization in the form of RGB percentages variation over the concentration is displayed in **Supplementary Figure S1c**. The response time of the protein sensor was 15 s at concentrations of 2.0, 4.0, and 6.0 mg mL^{-1} (**Figure 4e**). The corresponding reflection spectra are shown in **Supplementary Figure S5**. Exposure to UV light at 355 nm showed good stability and reliability of the sensor up to 30 minutes (**Figure 4f, Supplementary Figure S2c**).
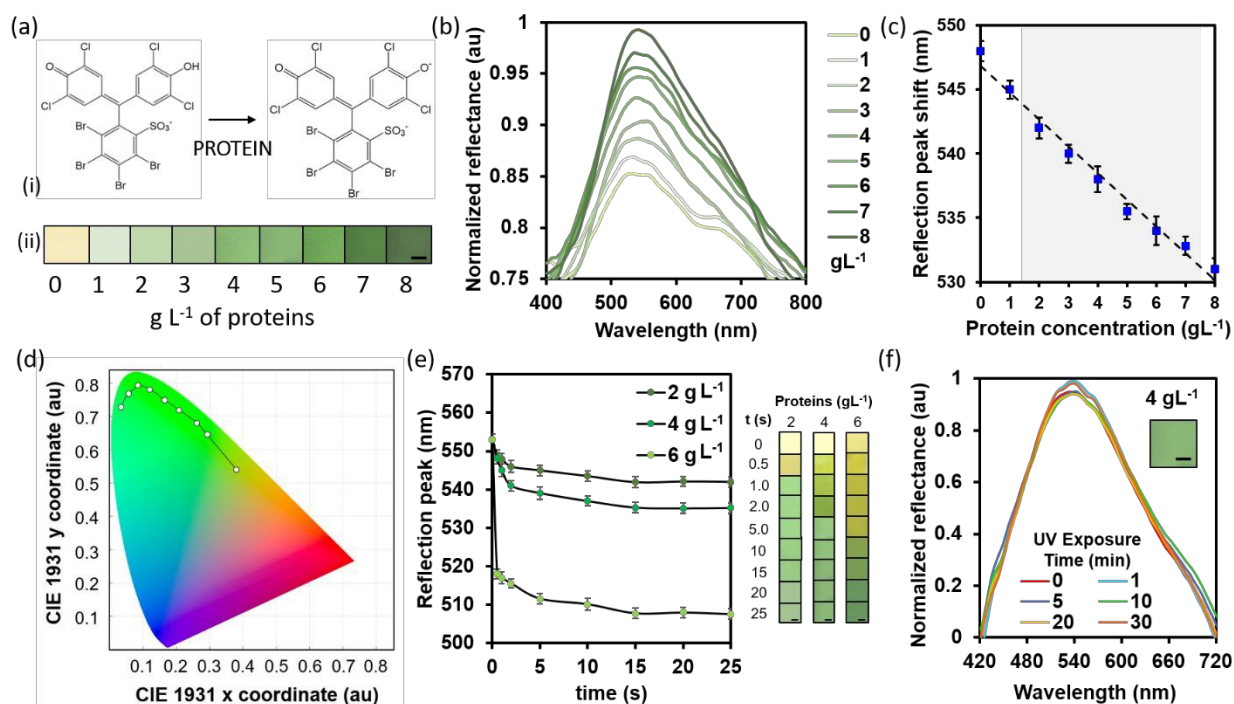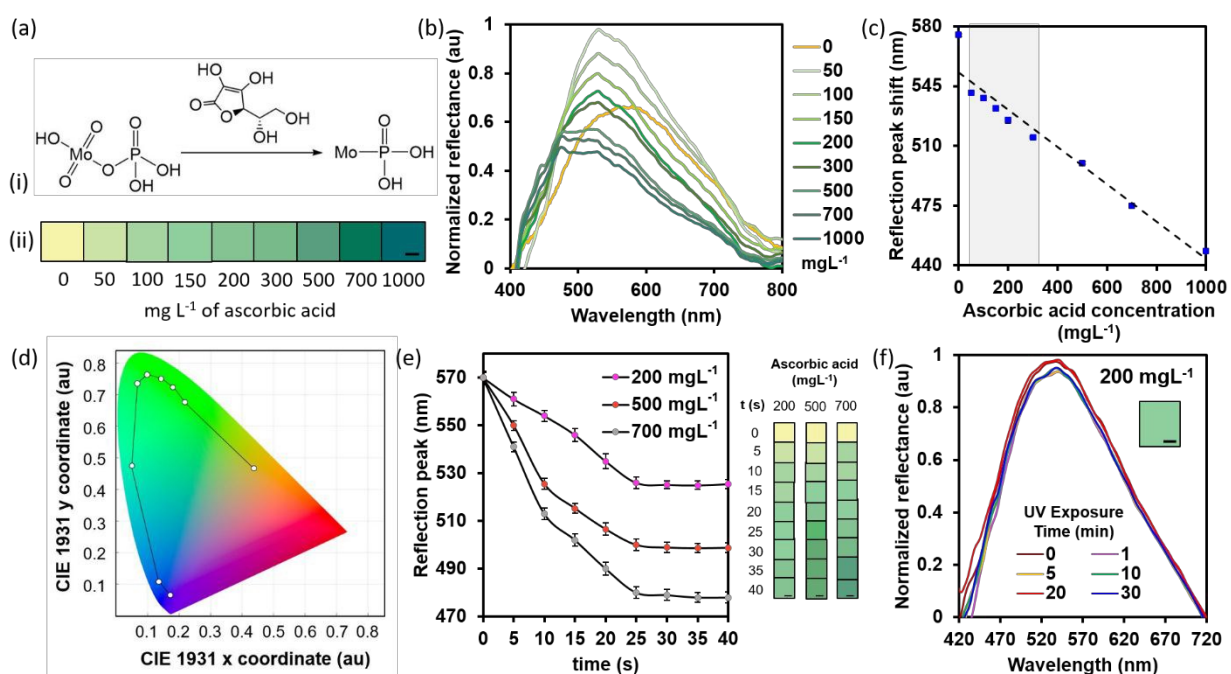

Figure 4. *Characterization of the paper tear protein sensor in the range between 0 and 8.0 mg mL^{-1}. (a) Sensing mechanism of proteins; (i) 3',3'',5',5''-tetrachlorphenol- 3,4,5,6-tetrabromsulfophthalein reacts with proteins to form an anion of the compound; (ii) Photographs of the chromogenic sensor;* scale bar: 1.5 mm. *(b) Normalized reflection spectra of the protein*

sensor at different concentrations; (c) Calibration curve of the protein sensor (with the grey area highlighting the normal physiological range); (d) Chromaticity diagram of the protein sensor, displaying the color change with protein concentration from 0 to 8.0 mg mL^{-1}. (e) Time-dependent reflection peak shift when exposed to 2.0, 4.0 and 6.0 mg mL^{-1} protein solutions. The inset displays the color shift. Scale bars: 1.0 mm. (f) UV-dependent behavior of the protein sensor at a protein concentration of 5.0 mg mL^{-1}. Inset scale bar: 1.5 mm.

L-ascorbic acid sensors (**Figure 5**) were based on the reduction of phosphomolybdic acid to phosphomolybdenum, to produce a color shift from yellow to green and blue, in the presence of 0-1.0 g L^{-1} of ascorbic acid (**Figure 5a**). **Figure 5b** shows the reflection spectra of the ascorbic acid sensor, with a calibration curve that could be approximated with a linear fitting (R^2=0.97) in the physiological range 50.0-300.0 mg L^{-1} (**Figure 5c**), from which a sensitivity of 0.05 nm/mgL^{-1} and a LOD of 59 mgL^{-1} were calculated. The CIE 1931 chromaticity diagram in **Figure 5d** displays the calibration points, i.e. the color coordinates corresponding to the sensor at nitrites concentrations ranging from 0 to 160 µmol L^{-1}. The smartphone RGB characterization of the colorimetric response is presented in **Supplementary Figure S1d**. Ascorbic acid sensors had a time response of 25 s which was

experimentally evaluated at concentrations of 200, 500 and 700 mg L^{-1} (**Figure 5f,**

Supplementary Figure S6). No degradation of the sensors was observed after UV

exposure for up to 30 minutes (**Figure 5e, Supplementary Figure S2d**).

Figure 5. *Characterization of the paper tear L-ascorbic acid sensor in the range between*

0 and 1.0 g L^{-1}: (a) Sensing mechanism of L-ascorbic acid: (i) Reduction of

phosphomolybdic acid to phosphomolybdenum in the presence of L-Ascorbic acid; (ii)

Photographs of the chromogenic sensor; scale bar: 1.5 mm. (b) Normalized reflection

spectra of the L-ascorbic acid sensor at different concentrations: (c) Calibration curve of the L-ascorbic acid sensor (with grey area highlighting the physiological range); (d) Chromaticity diagram of the L-ascorbic acid sensor, displaying the color change with L-ascorbic acid concentration from 0 to 1 gL^{-1}. (e) UV-dependent behavior of the L-ascorbic acid sensor at protein concentrations of 200, 500 and 700 mg L^{-1}. Inset scale bar: 1.5 mm. (f) Time-dependent reflection peak shift when exposed to a 200 mg L^{-1} L-ascorbic acid solution. Scale bar: 1.5 mm.

Tear nitrite sensors were based on the reaction of nitrite ions with sulfanilamide to form a diazonium salt, which further binds N-(1-naphthyl)- ethylenediamine dihydochloride (**Figure 6a**), to produce a pink azo dye, yielding a color shift from light yellow to fuchsia upon changing the concentration of nitrites from 0 to 160.0 μmol L^{-1} (Figure 5a, iii). The absorbance peak of the dye is measured at 528 nm. **Figure 6b** shows the reflection spectra of tear nitrite sensors, and **Figure 6c** depicts the calibration curve with linear fitting (R^2=0.92) in the range 80.0 -140.0 μmol L^{-1}. It yielded a sensitivity of 0.53 nm/μmolL^{-1} and

a LOD of 19.2 µmol L^{-1}. The CIE 1931 chromaticity diagram in **Figure 6d** displays the

calibration points, i.e. the color coordinates corresponding to the sensor at nitrites

concentrations ranging from 0 to 160.0 µmol L^{-1}. The smartphone RGB characterization

of the colorimetric response is presented in **Supplementary Figure S1e**. The nitrite sensor

had a time response of 20 s, which was experimentally evaluated at nitrites

concentrations of 40, 100 and 140 µmol L^{-1} (**Figure 6f**). The corresponding reflection

spectra over time are presented in **Supplementary Figure S5.** Nitrite sensors showed a

reliable behavior after up to 30 minutes of UV exposure (**Figure 6f, Supplementary Figure**

S7).
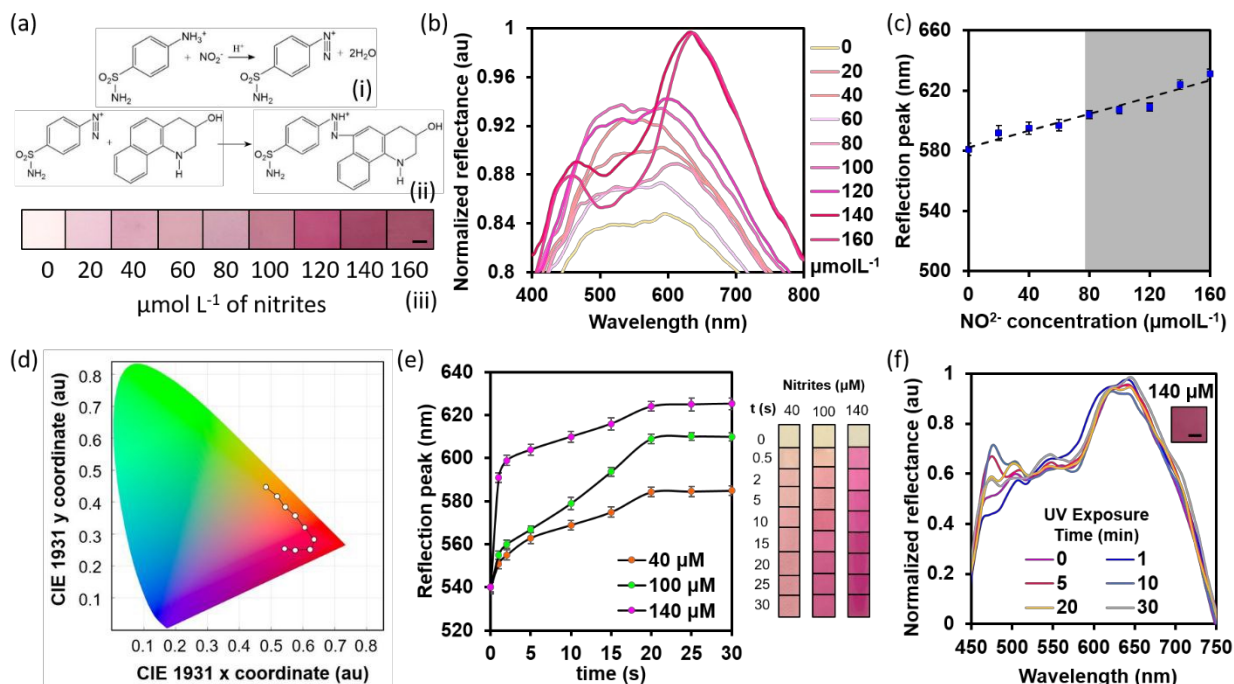
Figure 6. *Characterization of the paper tear nitrite sensor in the range between 0 and 160 µmolL⁻¹. (a) Sensing mechanism of nitrites: (i) Nitrite ions react with sulfanilamide to form a diazonium salt; (ii) the diazonium salt binds N-(1-naphthyl)- ethylenediamine dihydochloride, producing a pink dye; (iii) Photographs of the chromogenic sensor; scale bar: 1.5 mm. (b) Normalized reflection spectra of the nitrite sensor at different concentrations; (c) Calibration curve of the nitrite sensor (with the grey area highlighting the physiological range); (d) Chromaticity diagram of the nitrite sensor, displaying the color change with nitrite concentration from 0 to 160.0 µmolL⁻¹. (e) Time-dependent*

reflection peak shift of the sensor when exposed to a 140.0 µmolL^{-1} nitrite solution. The inset shows the color shift over time. Scale bars: 1.0 mm. (f) UV-dependent behavior of the nitrite sensor at a nitrite concentration of 140.0 µmolL^{-1}. Inset scale bar: 1.5 mm.

Paper microfluidic chips with different geometries were obtained by laser cutting. An interative process of testing resulted in an optimized design, able to host 1-2 µL of sample, with a wetting time of 1 to 2 s, as shown in **Figure 7a** (where an aliquot of 10.0 mM fluorescein solution was injected to quantify flow characteristics). These paper-based chemical sensors were embedded in the microfluidic system which were then sealed in place using a laboratory-made poly-HEMA contact lens, using acrylate chemical bonding (**Supplementary Figure S8**). Chemical sensors integrated into contact lenses were characterized and compared to free-standing sensors (**Figure 7b**). Consistent results were observed, with standard variations in the reflection peak of 1.7 nm for the pH sensor (**Figure 7b, i**), 2.1 nm for the ascorbic acid sensor (**Figure 7b, ii**), 2.3 nm for the glucose

sensor (**Figure 7b, iii**), 1.1 nm for the nitrite sensor (**Figure 7b, iv**), and 2.0 nm for the

protein sensor (**Figure 7b, v**).
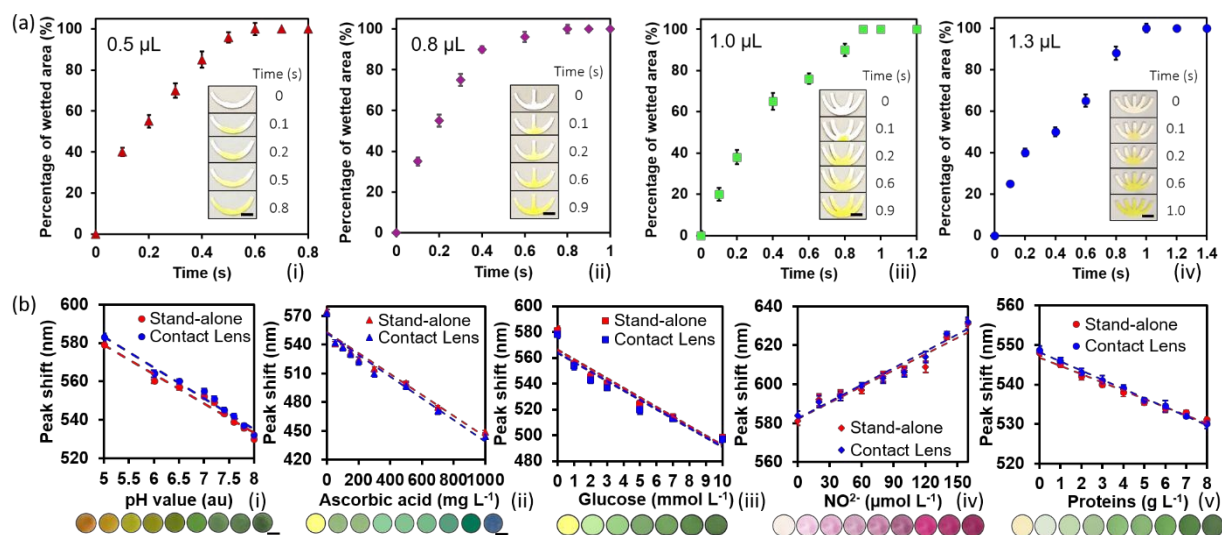
Figure 7. Capillary flow within the paper based microfluidic device and characterization of the tear fluid sensors embedded in the contact lenses. (a) Time characterization of capillary flow in paper based microchannels: (i) Two-branches channel, filled in 0.6 s with 0.5 μL of fluorescein solution: (ii) Three-branches channel, filled in 0.8 s with 0.8 μL of fluorescein solution; (iii) Four-branches channel, filled in 0.9 s with 1.0 μL of fluorescein solution: (iv) Five-branches channel, filled in 1.0 s with 1.3 μL of fluorescein solution. The scale bar of the insets is 3.0 mm. (b) Comparison of the reflection peak shift between the stand-alone and the contact lens-embedded sensor for (i) the pH sensor in the range of

5.0 to 8.0; (ii) the ascorbic acid sensor, in the range 0 to 1.0 g L^{-1}; (iii) the glucose sensor,

in the range 0 to 10.0 mmolL^{-1}; (iv) the nitrite sensor, in the range 0 to 160.0 μmolL^{-1}; and

(v) the protein sensor in the range 0 to 8.0 mg mL^{-1}. The scale bar of the insets is 1.5 mm.

A bespoke Tears Diagnostics smartphone application prototype was designed using

Visual Studio tools Mobile App Net development in Xamarin forms. A customized readout

device was designed which comprised a metallic *black box* with a front opening for the

smartphone camera (**Figure 8a**). **Figure 8b** displays the ease of operation for the readout

device. An image was either obtained before or whilst running the app. An example of an

image to processes is displayed in **Figure 8c**. The use of a readout device allows for a

higher readout precision, by minimizing the noise contribution given by ambient light

fluctuations. The sensors were imaged under smartphone light only, at the same, normal

angle of irradiation (90°). An example of readout is illustrated in **Figure 8d-k**, displaying

the working principle of Tears Diagnostics app.

The smartphone application (App) prototype was generated using Visual Studio Xamarin

Forms on a virtual machine running Android on a Samsung Galaxy S10. The code logic

was based on the nearest neighbour model, already validated for color detection in dye-based

sensors.[35] The algorithm was expanded to the multiplexed readout of pH, glucose, proteins,

ascorbic acid and nitrite ions. We excluded the need for a light calibration step by using a bespoke,

tailored readout device acting as a black box, to filter out the noise contribution given by ambient

lighting.

Upon opening the app, the user is asked to insert their name (**Figure 8d**), which is

accepted (**Figure 8e**) and the main menu of the app pops up, where the user can select

to take a measurement, update personal information, consult the reference values, or

check their medical records (**Figure 8f**). If "take measurement" was clicked, the user was

asked to either take or upload a photo (**Figure 8g**). In this example, the photograph of the

contact lens on an ex-vivo eye model is uploaded. The user was asked to select the

region of interest, by simply drawing a circle around the sensor to be measured and

indicating the analyte under measurement (**Figure 8h**). In this case, the pH sensor at the

far left was selected. The app read the color and outputs a pH value of 7.2 (**Figure 8i**),

based on the discrete calibration points defined in the nearest neighbor model. This

method had a 100% success on the discrete concentration values defined by the

developer, and it can be updated if new data points are inserted. **Figure 8j** and **Figure 8k**

display the "medical record" and "reference values" windows. The medical record can be

tracked in a calendar and sent to the healthcare professional. The reference values can

be compared to a selected measurement.
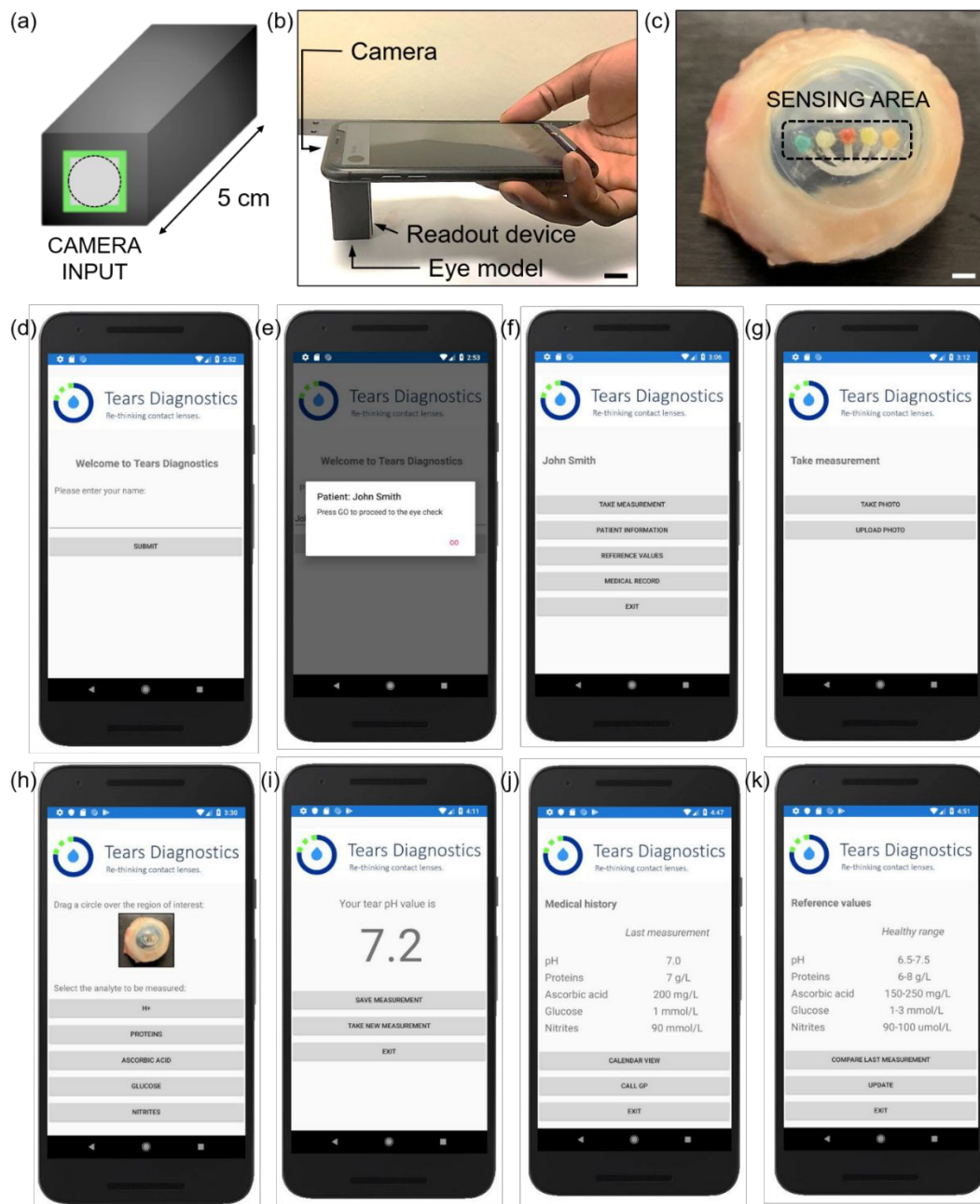
Figure 8. *Smartphone readouts of contact lens sensors. (a) Schematic of the readout*

device; (b) Readout of a contact lens sensor exposed to artificial tear fluid on an ex vivo

eye model; scale bar: 1.5 cm. (c) Photograph of the contact lens sensor inside the readout

device during a sustained artificial tear fluid flow on an ex vivo model; scale bar: 2.5 mm.

(d-k) Smartphone readouts; (d) The welcome page of the app; (e) The name of the patient is entered; (f) showing the App menu; (g) The take measurements section where the patient is asked to take or to upload a photo of the sensor; (h) The region of interest (ROI) and the corresponding analyte to be measured are selected; (i) The App outputs the concentration value associated with the analyte's color in the ROI; (j) Medical record section of the app, where the previous measurements may be saved; (k) Reference values section of the App. The healthy ranges of biomarkers were displayed and were compared to measurements. The response could be sent to a clinician or healthcare provider such as a General Pratictioner (GP).

Conclusions

Colorimetric sensors were synthetized before being deposited on paper, and then embedded as a paper microfluidic sensor within a commercial laser-inscribed acrylate contact lens. The microfluidic chip was sealed by chemically bonding a laboratory-made poly-HEMA contact lens. The paper sensors detected changes in the concentration of hydrogen ions (pH), ascorbic acid, glucose, proteins, and nitrite ions in 2 μL of artificial tear fluid within 35 s. The microfluidic chip could be filled in 1-2 s. All dye-based colourimetric sensors showed good stability when

investigated through UV exposure for up to 30 minutes. The smartphone application (App) was optimized for the multiplexed detection of analytes concentrations in a tear fluid model, by comparing the chromatic variations of the biosensors to its calibration points. The advantage of using paper-based sensors relied on the feasibility to operate the device without calibration on the eye color. The readout device acted as a *black box* in which the smartphone light source standardized the measurements by removing the noise contributions arising from the variation of color saturation and brightness under different lighting conditions. Sensors used in this study are not associated with toxicity concerns, due to their low concentrations and the fact that they are retained in a paper matrix, sealed in the lens. In future, the sensor feasibility should be assessed in *in vivo* samples and in *in vitro* animal models to understand the immunogenicity and foreign body response. In addition, the platform may be suited to detect a variety of electrolytes, cytokines, pathogenic microorganisms and other biomarkers, which may have possible applications in medical diagnostics to monitor a broad range of ocular conditions.

Materials and methods

Materials. Deionized water, D-(+)-glucose (99.5%), L-ascorbic acid, $NaNO_3$, KCl, NaCl, urea, citric acid, protein standard (200 mg mL^{-1}), HEMA, 2-hydroxy-2-methylpropiophenone, ethylene glycol dimethacrylate, bromothymol blue, methyl red, and phenolphthalein, glucose oxidase, peroxidase, and 3,3',5,5'-tetramethylbenzidine, phosphomolybdic acid, 3',3'',5',5''- tetrachlorophenol- 3,4,5,6- tetrabromosulfophthalein, sulfanilamide, N-(1-

naphthyl)- ethylenediamine dihydochloride, 3-aminopropyltriethoxysilane, 3-glycidoxypropyltriethoxysilane, Tris HCl, Tris base, sodium fluorescein, and phosphate buffered saline (PBS) tablets were purchased from Sigma-Aldrich and used with no additional purification. Filter paper was purchased from Fisher Scientific. Commercial contact lenses based on Boston XO (fluorosilicone acrylate) material were supplied by No7 Contact Lenses, UK.

Laser inscription of acrylate contact lenses and laser cutting of paper microfluidic systems.

Microfluidic patterns were designed on CorelDraw and further inscribed in commercial acrylate contact lenses using a CO_2 Rayjet laser system, operating at a wavelength of 11.6 μm, with a speed of 60% and a power of 50%. The material thickness was set to 100 μm. The same software and equipment were used to design paper microfluidic chips via CO_2 laser cutting, at power a laser power of 80%, scanning speed of 90%, and thickness of 200 μm.

Preparation of chemical sensors.

The pH sensor was synthesized using bromothymol blue (50.0 µg), methyl red (5.0 µg) and phenolphthalein (25.0 µg). The glucose sensor was prepared diluting 3,3',5,5'-tetramethylbenzidine (250.0 µg), GOD (25 U) and POD (120 U) in DI water. The protein sensor contained 3',3'',5',5''-tetrachlorophenol-3,4,5,6-tetrabromosulfophthalein (20.0 µg). The nitrite sensor contained 3-hydroxy-1,2,3,4-tetrahydro-7,8-benzoquinoline (50.0 µg) and sulfanilamide (40 µg). The L-ascorbic acid sensor contained phosphomolybdic acid (100.0 µg). The liquid-state sensors were deposited on paper circles with a diameter of 2.0 mm, and air-dried.

Fabrication of poly-HEMA contact lenses.

HEMA (95 vol/vol %), the photoinitiator 2-hydroxy-2-methylpropiophenone (1 vol/vol %), and the cross-linker ethylene glycol dimethacrylate (4 vol/vol %) were mixed, pipetted into a contact lens mold, and cured under UV light ($\lambda = 365$ nm) for 5 min.

Poly-HEMA to acrylate chemical bonding.

As a first step, -OH groups are obtained on both surfaces (poly-HEMA and fluorosilicone acrylate) by activating them via O_2 plasma for 1 minute at 60W, using a Henniker Plasma

System. Subsequently, the poly-HEMA lens is soaked in a 1:100 (v/v) 3-aminopropyltriethoxysilane (APTES) aqueous solution and the acrylate lens is soaked in a 1:100 (v/v) 3-glycidoxypropyltriethoxysilane (GPTES) aqueous solution for 20 minutes. The lenses are then rinsed in deionized water, and air-dried. The surfaces are now ready to be brought into contact applying a slight pressure, after depositing the microfluidic paper in the acrylate contact lens.

Preparation of artificial tear fluid.

Artificial tear fluid contained NaCl (125.0 mmol L^{-1}), KCl (20.0 mmol L^{-1}), urea (5.0 mmol L^{-1}), citric acid (31.0 μmol L^{-1}), L-ascorbic acid (0-1.0 g L^{-1}), $NaNO_2$ (0-160.0 μmol L^{-1}), glucose (0-10.0 mmol L^{-1}), albumin (0-8.0 g L^{-1}), and the pH value was adjusted to 5.0 - 8.0 using Tris HCl and Tris base.

Readout method.

A customized smartphone application (App) prototype was developed using the module Mobile app.net with Xamarin forms on Visual Studio, running a virtual Samsung Galaxy

S10 with Android 5.0. Each sensor was calibrated with a discrete number of colors, given

by photographs of the sensors exposed to solutions having known concentrations of each

analyte, which served as inputs to the algorithm. Colorimetric changes were captured by

the complementary metal-oxide-semiconductor (CMOS) sensor equipped in a

smartphone camera. Upon detection, concentration values were assigned to the captured

images, based on the nearest neighbor model, i.e. the algorithm compared the newly

captured color to the calibration colors of the sensor of interest, by converting it to (x, y)

coordinates in the CIE 1931 chromaticity diagram, and returning the concentration value

corresponding to "nearest neighbouring" calibration color in the plot. This method allowed

to have a 100% success rate over the discrete number of values defined during the

calibration of the App. This concept could be expanded by increasing the number of

calibration points, as well as by coupling it to a machine learning algorithm that could be

able to estimate intermediate values between consecutive calibration points.

ASSOCIATED CONTENT

Supplementary information

Supplementary information can be found in a separate file.

AUTHOR INFORMATION

Corresponding Author

*r.moreddu18@imperial.ac.uk

Author contributions

R.M. and A.K.Y. conceived the idea. R.M. performed the experiments and wrote the manuscript. All authors gave insights on the work and reviewed the manuscript.

Funding sources

Conflict of Interest

R.M. founded the spin-off company Tears Diagnostics.

ACKNOWLEDGMENT

REFERENCES

1.   D. C. Christodouleas, B. Kaur and P. Chorti, *ACS Cent Sci*, 2018, **4**, 1600-1616.

2.   M. Elsherif, R. Moreddu, M. U. Hassan, A. K. Yetisen and H. Butt, *Lab Chip*, 2019, **19**, 2060-2070.

3.   R. Moreddu, M. Elsherif, H. Butt, D. Vigolo and A. K. Yetisen, *RSC Advances*, 2019, **9**, 11433-11442.

4.   A. K. Yetisen, R. Moreddu, S. Seifi, N. Jiang, K. Vega, X. Dong, J. Dong, H. Butt, M. Jakobi, M. Elsner and A. W. Koch, *Angew Chem Int Ed Engl*, 2019, DOI: 10.1002/anie.201904416.

5.   R. S. Riaz, M. Elsherif, R. Moreddu, I. Rashid, M. U. Hassan, A. K. Yetisen and H. Butt, *ACS Omega*, 2019, **4**, 21792-21798.

6.   X. Yang, X. Pan, J. Blyth and C. R. Lowe, *Biosens Bioelectron*, 2008, **23**, 899-905.

7.   R. Moreddu, J. S. Wolffsohn, D. Vigolo and A. K. Yetisen, *Sensors and Actuators B: Chemical*, 2020, **317**.

8.   M. E. Stern, R. W. Beuerman, R. I. Fox, J. Gao, A. K. Mircheff and S. C. Pflugfelder, *Cornea*, 1998, **17**, 584-589.

9.   R. Moreddu, D. Vigolo and A. K. Yetisen, *Adv Healthc Mater*, 2019, DOI: 10.1002/adhm.201900368, e1900368.

10.   R. Ihnatko, U. Eden, N. Lagali, A. Dellby and P. Fagerholm, *J Proteomics*, 2013, **94**, 78-88.

11.   J. Soria, J. A. Duran, J. Etxebarria, J. Merayo, N. Gonzalez, R. Reigada, I. Garcia, A. Acera and T. Suarez, *J Proteomics*, 2013, **78**, 94-112.

12.   S. J. Venkata, A. Narayanasamy, V. Srinivasan, G. K. Iyer, R. Sivaramakrishnan, M. Subramanian and R. Mahadevan, *Indian J Ophthalmol*, 2009, **57**, 289-292.

13.   N. A. Delamere, *Subcell Biochem*, 1996, **25**, 313-329.

14.   R. N. Williams and C. A. Paterson, *Exp Eye Res*, 1986, **42**, 211-218.

15.   S. Saika, K. Uenoyama, K. Hiroi, H. Tanioka, K. Takase and M. Hikita, *Graefes Arch Clin Exp Ophthalmol*, 1993, **231**, 221-227.

16.   N. Kasetsuwan, F. M. Wu, F. Hsieh, D. Sanchez and P. J. McDonnell, *Arch Ophthalmol*, 1999, **117**, 649-652.

17.   M. B. Abelson, I. J. Udell and J. H. Weston, *Archives of Ophthalmology*, 1981, **99**, 301-301.

18.   L. G. Carney, T. F. Mauger and R. M. Hill, *Acta Ophthalmologica*, 1990, **68**, 75-79.

19.   M. B. Abelson, A. A. Sadun, I. J. Udell and J. H. Weston, *American Journal of Ophthalmology*, 1980, **90**, 866-869.

20.   J. E. M. Thygesen and O. L. Jensen, *Acta Ophthalmologica*, 1987, **65**, 134-136.

21.   G. E. K. Mirza, S.; Er, M.; Güngörmüs, N.; Karaküçükb, I.; Saraymen, R., *Ophthalmic research*, 2001, **33**, 48-51.

22.   J. D. Lane, D. M. Krumholz, R. A. Sack and C. Morris, *Current Eye Research*, 2006, **31**, 895-901.

23.   J. Zhang, W. Hodge, C. Hutnick and X. Wang, *J Diabetes Sci Technol*, 2011, **5**, 166-172.

24.   C. Chen, Z.-Q. Dong, J.-H. Shen, H.-W. Chen, Y.-H. Zhu and Z.-G. Zhu, *ACS Omega*, 2018, **3**, 3211-3217.

25.   J. L. Ruan, C. Chen, J. H. Shen, X. L. Zhao, S. H. Qian and Z. G. Zhu, *Polymers (Basel)*, 2017, **9**, 125.

26.   V. L. Alexeev, S. Das, D. N. Finegold and S. A. Asher, *Clin Chem*, 2004, **50**, 2353-2360.

27.   S. Manju, P. R. Hari and K. Sreenivasan, *Biosens Bioelectron*, 2010, **26**, 894-897.

28.   M. Elsherif, M. U. Hassan, A. K. Yetisen and H. Butt, *ACS Nano*, 2018, **12**, 5452-5462.

29.   H. Yao, A. J. Shum, M. Cowan, I. Lahdesmaki and B. A. Parviz, *Biosens Bioelectron*, 2011, **26**, 3290-3296.

30.   H. Y. Yu-Te Liao, Andrew Lingley, Babak Parviz, Brian P. Otis, *IEEE Journal of Solid-State Circuits* 2012, **47**.

31.   H. Yao, Y. Liao, A. R. Lingley, A. Afanasiev, I. Lahdesmaki, B. P. Otis and B. A. Parviz, *Journal of Micromechanics and Microengineering*, 2012, **22**.

32.   S. Iguchi, H. Kudo, T. Saito, M. Ogawa, H. Saito, K. Otsuka, A. Funakubo and K. Mitsubayashi, *Biomedical Microdevices*, 2007, **9**, 603-609.

33. E. F. Gabriel, P. T. Garcia, T. M. Cardoso, F. M. Lopes, F. T. Martins and W. K. Coltro, *Analyst*, 2016, **141**, 4749-4756.

34. A. K. Yetisen, N. Jiang, A. Tamayol, G. U. Ruiz-Esparza, Y. S. Zhang, S. Medina-Pando, A. Gupta, J. S. Wolffsohn, H. Butt, A. Khademhosseini and S. H. Yun, *Lab on a Chip*, 2017, **17**, 1137-1148.

35. A. K. Yetisen, J. L. Martinez-Hurtado, A. Garcia-Melendrez, F. da Cruz Vasconcellos and C. R. Lowe, *Sensors and Actuators B: Chemical*, 2014, **196**, 156-160.

Lab on a Chip Accepted Manuscript
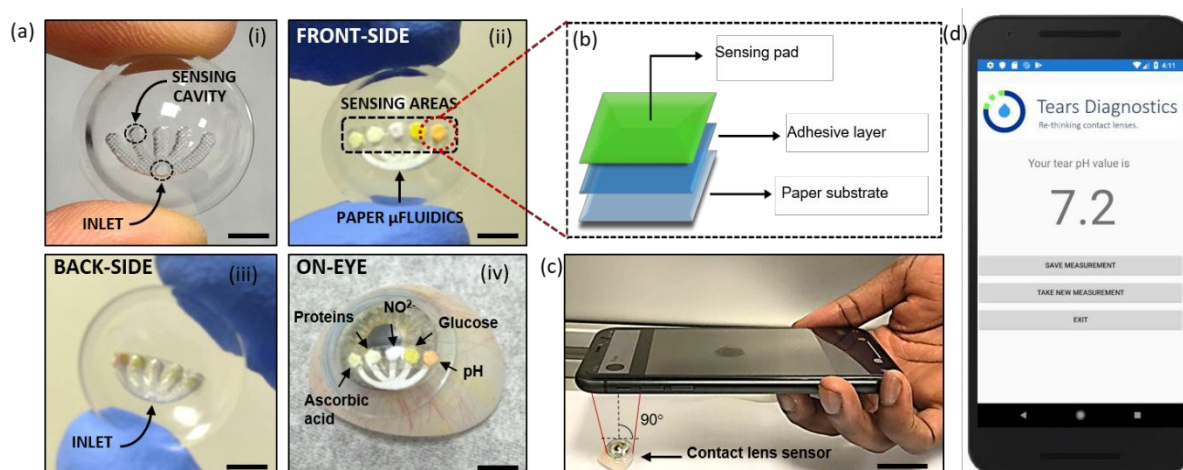
Lab on a Chip Accepted Manuscript

Lab on a Chip
Table of contents

Title: Integration of Paper Microfluidic Sensors into Contact Lenses for Tear Fluid

Analysis

Authors: Rosalia Moreddu, Mohamed Elsherif, Hadie Adams, James S. Wolffsohn,

Daniele Vigolo, Haider Butt, Jonathan M. Cooper, Ali K. Yetisen

Paper microfluidic sensors were integrated into laser-inscribed contact lenses to allow smartphone-assisted screening of tear metabolites to aid ocular diagnostics.

Lab on a Chip Accepted Manuscript